CrystEngComm

COMMUNICATION

View Article Online
View Journal | View Issue

Cite this: *CrystEngComm*, 2017, **19**, 2294

Received 1st March 2017,
Accepted 30th March 2017

DOI: 10.1039/c7ce00428a

rsc.li/crystengcomm

Epitaxial growth of wafer-scale two-dimensional polytypic ZnS thin films on ZnO substrates

Lei Wang,[ab] Kanglin Xiong,[c] Yangkun He,[d] Xing Huang,[ae] Jing Xia,[a] Xuanze Li,[ab] Yiyi Gu,[ab] Huaqiu Cheng[ab] and Xiangmin Meng *[a]

In this paper, we report the first successful epitaxial synthesis of flat wafer-scale two-dimensional ZnS thin films on single-crystalline ZnO substrates with high reproducibility, stability, and reliability, despite the large lattice mismatch (approximately 20%) between ZnO and ZnS. The as-grown ZnS was composed of two crystal phases: wurtzite (WZ) and zinc blende (ZB). The epitaxial orientation between the different phases was identified as: [2–1–10] ZnO_{WZ}//[2–1–10] ZnS_{WZ}//[10–1] ZnS_{ZB} and (0001) ZnO_{WZ}// (0001) ZnS_{WZ}//(111) ZnS_{ZB}. The crystal structure and the strain profile at the interfaces were studied in detail. After a simple etching treatment, exfoliated large-area free-standing ZnS thin films were achieved for the first time. The present product is expected to become valuable to the strategy of growing large-area thin films or heterostructures with a large lattice mismatch.

Introduction

Large-area semiconductor thin films serve as the basis for modern electronics and optoelectronics.[1] They have found practical applications in a wide variety of fields including solar cells,[2] integrated circuits,[3] solid-state lighting,[4] and sensors.[5] During the past decades, various routes, such as magnetic sputtering,[6] atomic layer deposition (ALD),[7] molecular beam epitaxy (MBE),[8] and metal organic chemical vapor deposition (MOCVD),[9] have been developed to synthesize semiconductor thin films. Among these strategies, of particular importance are the ones that are able to grow single-crystalline or polytypic thin films epitaxially. Single-crystalline and polytypic semiconductor thin films are promising due to their assistance in interface electron scattering reduction and device performance improvement compared to their corresponding amorphous or polycrystalline counterparts.[10] However, the residual elastic strain between the film and the substrate is a critical obstacle that needs to be overcome.[11–14] Excessive strains would lead to the rolling up or cracking of the films, and subsequent malfunction of the components in application.

Zinc sulphide (ZnS) is one of the first semiconductor materials ever discovered, and is considered to be a highly promising building block for novel diverse applications,[15] such as ultraviolet light emitting diodes,[16] photodetectors,[17] flat panel displays,[18] thin films solar cells,[19] *etc.* ZnS has two structural forms – cubic sphalerite and hexagonal wurtzite, with large direct band gaps of 3.72 eV and 3.77 eV,[10,13,20,21] respectively, making it an ideal alternative to the cadmium-free $Cu(In,Ga)Se_2$ (CIGS) buffer layer.[19] The difference between the two structures is the sequence of atomic layer stacking parallel to {111} for cubic or {0001} for hexagonal planes in the form of ABCABC or ABAB. Many theoretical and experimental efforts have been devoted to the fabrication of ZnS materials,[22–27] particularly those formed in a two-dimensional manner that enables integrated fabrication and application of ZnS-based optoelectronic devices, and may also bring about some unique properties and functions.[28–31] However, the synthesis of large-area ZnS thin films with high crystal quality still remains challenging.[32] This is due to the lack of a lattice-matched substrate, the oxidation propensity, and the high sensitivity to synthetic conditions of ZnS.[10] ZnO is sometimes used as the substrate to grow ZnS materials.[23,33] However, there exists a very large intrinsic lattice mismatch between wurtzite ZnO and wurtzite ZnS (20% for plane (0001) and 18% for plane (01–10)) which makes it quite difficult to epitaxially grow large-area uniform single-crystalline ZnS films on a ZnO substrate.

Considering the great interest in achieving large-area ZnS thin films, here we developed a novel chemical vapor

[a] *Key Laboratory of Photochemical Conversion and Optoelectronic Materials, Technical Institute of Physics and Chemistry, Chinese Academy of Sciences, Beijing 100190, PR China. E-mail: mengxiangmin@mail.ipc.ac.cn*
[b] *University of Chinese Academy of Sciences, Beijing 100039, PR China*
[c] *Department of Electrical Engineering, Yale University, New Haven, Connecticut 06520, USA*
[d] *School of Materials Science and Engineering, Beihang University, Beijing 100191, PR China*
[e] *Department of Inorganic Chemistry, Fritz Haber Institute of the Max Planck Society, Faradayweg 4-6, 14195 Berlin, Germany*

deposition epitaxial synthesis of wafer-scale ZnS thin films with a thickness of less than 30 nm on bulk single-crystalline ZnO substrates. The detailed crystal structure was systematically investigated. Graphical phase analysis was conducted to study the interface stresses between the different crystal phases. Furthermore, a simple etching process was used to etch away the ZnO substrate and large-area free-standing ZnS thin films were achieved, for the first time. Our study opens a new window for heterostructures with a huge lattice mismatch.

Experimental

Synthesis process

The synthesis of the wafer-scale ZnO/ZnS heterostructure was carried out in a high temperature tube furnace with two heating zones *via* a thermal deposition method. The diameter of the quartz tube is 3 cm and the distance between the two heating zones is 50 cm. ZnS powder and ZnO bulk single crystal with the polished side facing upwards were placed at the high-temperature zone and the low-temperature zone, respectively. Then, Ar was flowed into the tube at a constant flow of 50 sccm, and the pressure in the system was maintained at 10 Pa. The two zones of the tube were heated to 850 °C and 600 °C, respectively, and kept at those temperatures for 1 hour. After the tube was naturally cooled down to room temperature, ZnS films were evenly deposited on the ZnO single crystal surface.

Characterization

Scanning electron microscopy (SEM) and composition analysis of the sample were conducted on a Hitachi S-4800 SEM equipped with an energy dispersive X-ray spectrometer (EDX). The X-ray diffraction pattern was recorded on a Bruker D8 Focus powder X-ray diffractometer using Cu Kα radiation (λ = 1.5418 Å). The cross-section sample for transmission electron microscopy (TEM) was prepared by focused ion beam (FIB) microscopy. The atomic force microscopy (AFM) image was taken using an Asylum Research MFP 3D. The microstructure of the heterostructures was investigated using a JEOL JEM-2100F operated at 200 kV. The atomic level strain is visualized by geometric phase analysis (GPA).

Results and discussion

Fig. 1a illustrates the schematic experimental setup for the synthesis process. Specifically, a <0001> oriented ZnO bulk single crystal serves as the substrate. The ZnS film is then grown on the ZnO substrate *via* thermal vaporization of ZnS powder. More details can be found in the experimental section. Fig. 1b and c show the top-view low-magnification and high-magnification SEM images of the as-synthesized products, respectively. It can be clearly seen that the film has a large area and a relatively smooth surface. As exhibited in Fig. 1d, the EDS spectrum reveals the presence of Zn, O, and S elements in the sample, indicating that ZnS has been successfully deposited on the ZnO single crystal. The weaker sulphur signal *versus* oxygen is possibly due to the small thickness of the ZnS film. Fig. 1e shows the AFM image of the sample. The root mean square (rms) roughness was found to be 0.358 nm, indicating the good surface quality of the film.

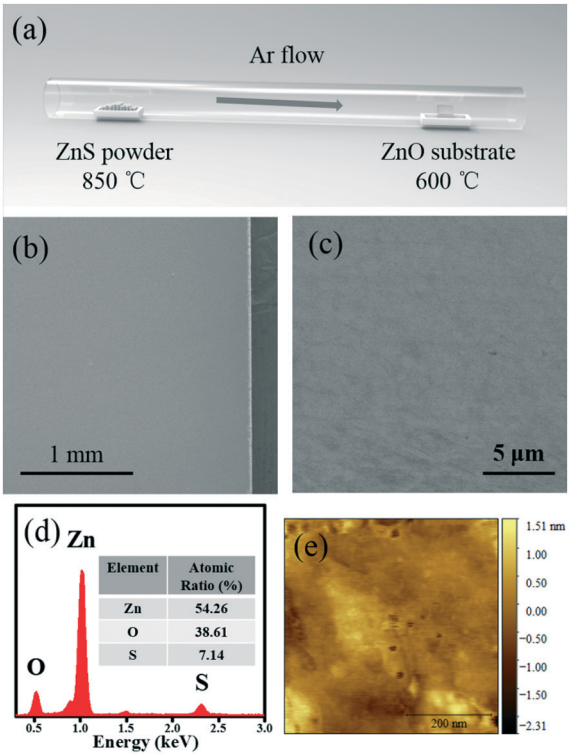

Fig. 1 (a) Schematic setup for the deposition of ZnS films on ZnO bulk single crystals; top-view (b) low-magnification and (c) high-magnification SEM images of the as-synthesized products; (d) EDS spectrum of the film; (e) AFM image of the film.

X-ray diffraction (XRD) measurement was performed to analyze the composition and phase structure of the products. As shown in Fig. 2a, the XRD spectrum of the ZnO/ZnS heterostructure was taken and compared to that of a ZnO single crystal. For the bare ZnO bulk single crystal, only a predominant diffraction peak at 34.4° and a relatively weak peak at 72.6° can be observed, which can be respectively indexed to the (0002) and (0004) planes of wurtzite ZnO (JPCDS, No. 36-1451). This results from the ZnO single crystal substrate growing along the *c*-axis. For the ZnO/ZnS product, a new

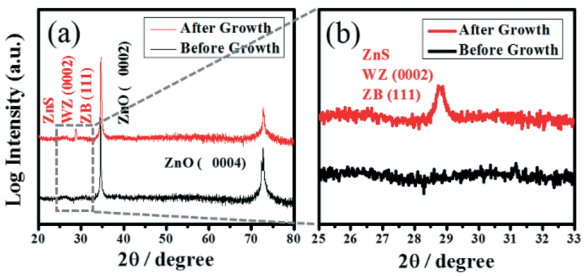

Fig. 2 (a) XRD pattern (on the log scale) of the samples; (b) XRD pattern of the marked region of (a).

diffraction peak at about 28.5° is detected (Fig. 2b). This peak can be indexed to either the (0002) plane of WZ ZnS (JPCDS, No. 36-1450) or the (111) plane of ZB ZnS (JPCDS, No. 05-0566) since these two peaks are indistinguishable from each other. Whichever the case, this is strongly indicative of the epitaxial growth of ZnS on ZnO. It is also noteworthy that the (0002) peak of ZnO is slightly blue shifted for the ZnO/ZnS sample. The blue shift originates from the larger lattice parameter of ZnS causing lattice constant expansion in ZnO.

To further investigate the structure and the crystal orientation of the sample, cross-section SEM, TEM, and selected-area electron diffraction (SAED) were employed. Fig. 3a demonstrates the fake color cross-section SEM image of the ZnO/ZnS heterostructure. It can be clearly observed that a large-area ZnS film (the top yellow layer) is uniformly grown on the ZnO substrate (the magenta layer). This eclipses what was reported previously that it is really difficult to grow large and uniform ZnS single-crystalline layers on ZnO substrates due to the large lattice mismatch between ZnS and ZnO.[13] Three layers with different contrasts, namely, the Au top layer, the ZnS middle layer, and the ZnO bottom layer, can be seen in the low-magnification cross-section TEM image of the ZnO/ZnS heterostructures (Fig. 3b). The Au layer was deposited on the sample for the purpose of protecting the materials underneath when focused ion beam (FIB) was utilized to prepare the TEM sample. A 28 nm-thick ZnS thin layer was evenly coated on the ZnO surface, not only on the top surface but also on the sidewall. Fig. 3c shows the cross-section HRTEM image of the interface between the ZnO layer and the upper layer. Located at the lower left is the ZnO layer. The lattice fringes of 0.52 nm correspond to the (0001) plane of WZ ZnO. Located at the upper right part of the image is a dual crystal phase compound. The measured interplanar distance of 0.62 nm (blue) and 0.31 nm (red) matches respectively with the (0001) crystal plane of WZ ZnS and (111) zinc blende (ZB) ZnS. The interfaces between each phase are atomically smooth. The corresponding SAED pattern (Fig. 3d) demonstrates 3 sets of well-aligned diffraction spots, which reveals an epitaxial relationship despite the large lattice mismatch, *i.e.*, [2–1–10] ZnO_{WZ}//[2–1–10] ZnS_{WZ}//[10–1] ZnS_{ZB} and (0001) ZnO_{WZ}//(0001) ZnS_{WZ}//(111) ZnS_{ZB}.

As we know, misfit dislocations often form in the epilayer to relieve the elastic strain associated with the mismatch of lattice constants and thermal expansion coefficients.[34,35] Considering that ZnO has a large intrinsic lattice mismatch with WZ ZnS (20% for plane (0001) and 18% for plane (01–10)) and also different crystal structures with ZB ZnS, there should be relatively large lattice distortions and a number of dislocations at the interface. Accurate lattice thickness determination, as well as Geometric Phase Analysis (GPA),[36] which uses the HRTEM data to extract displacement information and directly map a continuous strain distribution, is utilized to analyze the lattice distortion around the phase boundaries. Fig. 4a presents the HRTEM image of the phase interphases (the two white dotted lines). The lattice layer thicknesses for the rectangular region (Fig. 4b) are calculated based on Gaussian fitting. The evolution of the layer distance

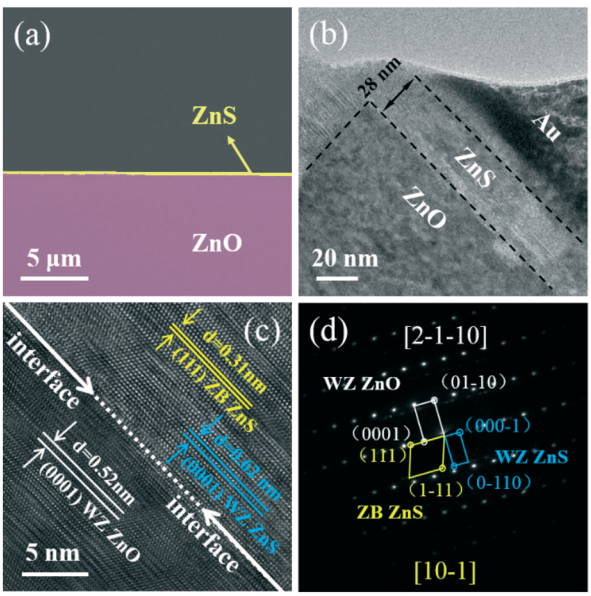

Fig. 3 Cross-section (a) SEM image (fake color) and (b) TEM image of the ZnO/ZnS film; (c) HRTEM image of the interface between the ZnO layer and ZnS layer; (d) corresponding selected-area electron diffraction pattern.

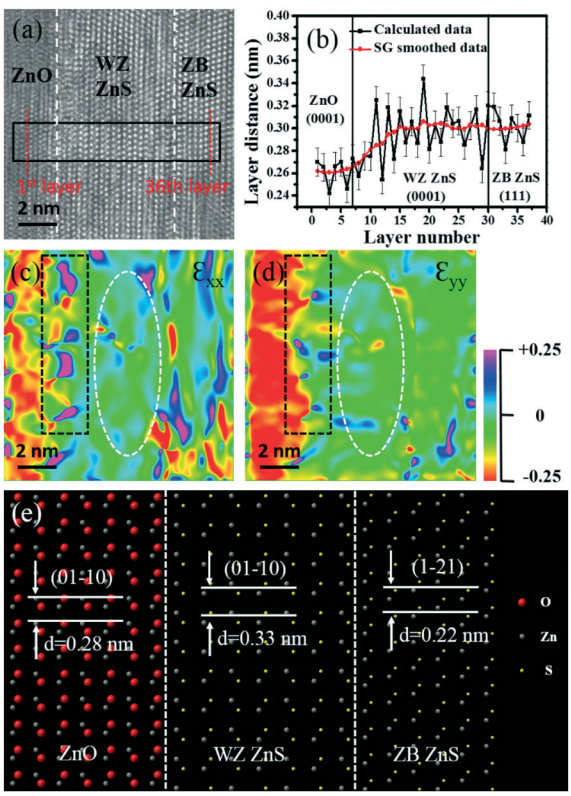

Fig. 4 (a) HRTEM image of the interfaces between different phases; (b) evolution of the layer distance of the heterostructure for the rectangular region in Fig. 4a; (c) distortion map along the [0001] direction; (d) distortion map along the [10–10] direction; (e) atomic model of the heterostructure interface.

after smooth processing indicates that the *d*-spacing of ZnO is 0.26 nm while those of WZ ZnS and ZB ZnS are both around 0.31 nm, coinciding well with the literature data. At the ZnO/WZ ZnS interface, the layer thickness increases gradually from 0.26 nm to 0.30 nm. The transition region contains 8 atomic layers in WZ ZnS. At the WZ ZnS/ZB ZnS interface, since the lattice constant of (0001) WZ ZnS is almost equal to that of (111) ZB ZnS, there is no obvious change in the layer thickness. Furthermore, it can be concluded that the lattice distortion in the WZ ZnS layer is larger than those in the ZnO layer and ZB ZnS layer because the deviation between the calculated layer thickness (black line) and the smoothed values (red line) in WZ ZnS is much greater. Fig. 4c and d show the GPA of the HRTEM image, and they visualize the distortion maps along the [0001] and [10–10] directions, respectively. WZ ZnS is chosen as the reference frame. The dislocations with an interval of about 5 atomic layers distribute at the ZnO/WZ ZnS interface, and they both exist along the [0001] and [10–10] directions (the boxed region). This is due to the fact that the interplanar distance of WZ ZnS is approximately 20% larger than that of ZnO, corresponding to 5 ZnO atomic layers. It can also be discovered that the compressive strain along the [01–10] direction in the WZ ZnS layer (the elliptical region) is larger than that along the [0001] direction. This is because the area of the film is so large that the strain generated along the substrate surface cannot be relieved. Another interesting phenomenon is that there are few dislocations at the WZ ZnS/ZB ZnS interface, especially along the [01–10] direction (in parallel to the substrate surface). This may be ascribed to the small thickness of the ZB ZnS layer, which doesn't exceed the critical thickness, and accordingly, the dislocation formation is not energetically favorable.[37]

ZnS, as a promising wide band gap material, has never been fabricated in the form of a wafer-scale two-dimensional membrane. In order to address this challenge and selectively remove the underlying ZnO sacrificial layer within a reasonable time, a periodic array of via-holes were created by inductively coupled plasma (ICP) on the ZnO/ZnS heterostructure surface, as shown in Fig. 5a. The holes are squares with a dimension of 10 μm. After rinsing the patterned sample in dilute acetic acid solution, the ZnO substrate was dissolved and the ZnS membrane became exfoliated. Fig. 5b presents the enlarged SEM image of the ZnS membrane which has a very curved morphology. The curved shape was due to the large residual stress in the ZnS layer. Present in Fig. 5c is the HRTEM image of the ZnS membrane viewed along [0001] of WZ ZnS or [111] of ZB ZnS. The labelled lattice spacings of 0.33 nm and 0.19 nm correspond to the (10–10) plane and (2–1–10) plane of WZ structured ZnS, respectively. This indicates that the exposed surface is WZ ZnS. Fig. 5d shows the corresponding SAED pattern. The well-arranged diffraction spots with six-fold symmetry confirm the good crystal quality of the membrane. The inner hexagonal spots correspond to the {–1100} planes of WZ ZnS, and the outer hexagonal spots can be indexed to the {2–1–10} planes of WZ ZnS. Of particular note is the brightness contrast between the two sets of spots. The outer six spots are much brighter than the inner ones. Considering the polytype nature, the epitaxial orientation relationship, and the lattice parameters of ZnS, the outer set of spots can also be indexed to the {2–20} planes of ZB ZnS, since there is a crystal orientation relationship of (2–1–10)WZ ZnS//(1–10)ZB ZnS (this has been discussed earlier), plus, the *d*-spacings of the WZ ZnS (2–1–10) plane and the ZB ZnS (2–20) plane are both 0.19 nm. This interesting relationship is also evidenced by the SAED model of the two structures. As shown in Fig. 5e and f, the diffraction spots of the two planes coincide well with each other. The above analysis confirms that the as-synthesized ZnS has the structure of alternating WZ/ZB stackings, which may provide the possibility of its application in charge-separation areas, other than the pre-mentioned areas, since WZ ZnS and ZB ZnS form a staggered type-II band alignment.[21,38,39]

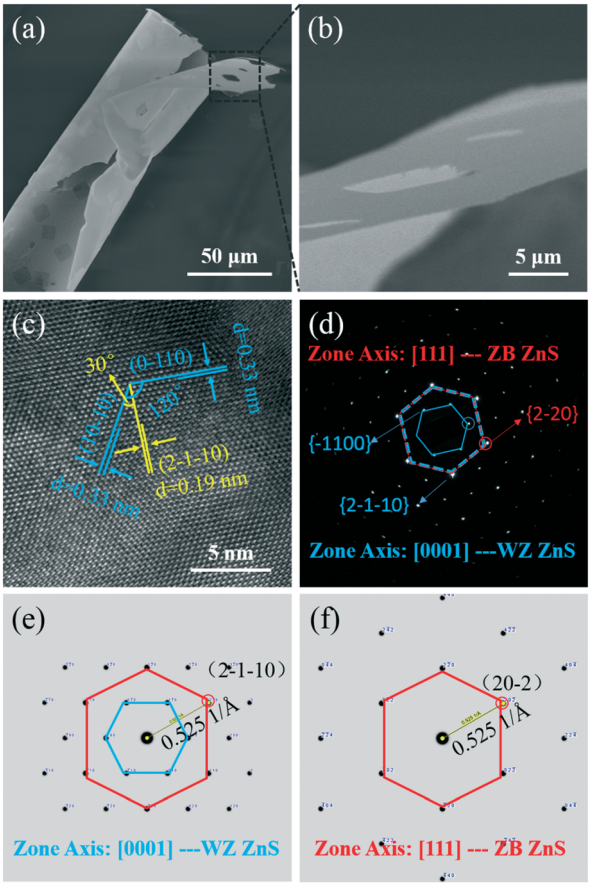

Fig. 5 (a) SEM image of the ZnS membrane ripped off from the ZnO substrate; (b) zoomed-in SEM image of the square area; (c) HRTEM image of the exfoliated ZnS nanomembrane; (d) corresponding SAED pattern; (e) SAED model of WZ ZnS with the zone axis of [0001]; (f) SAED model of WZ ZnS with the zone axis of [111].

Conclusions

The challenging epitaxial synthesis of wafer-scale ZnS thin films on ZnO substrates has been successfully achieved

through a novel CVD method, for the first time. TEM images reveal that ZnS is composed of two crystal structures: wurtzite and zinc blende. The epitaxial relationship is identified to be [2–1–10] ZnO_{WZ}//[2–1–10] ZnS_{WZ}//[10–1] ZnS_{ZB} and (0001) ZnO_{WZ}//(0001) ZnS_{WZ}//(111) ZnS_{ZB}. The microstructure and the interface stress have been studied systematically. By immersing the samples into a dilute acid solution, the ZnO substrate is dissolved and large-area ZnS thin films with high crystal quality are produced for the first time. The as-synthesized heterostructure and the ZnS thin film may find applications in versatile areas. Also, the growth strategy may provide a powerful synthesis platform for other material systems.

Acknowledgements

This work was financially supported by the "Strategy Priority Research Program" of the Chinese Academy of Sciences (Grant No. XDA09040203) and 973 Project (2012CB932401). Dr. Lei Wang would like to thank the funding from the "Graduate Candidate International Joint Training Program" of the Chinese Academy of Sciences during the period of 2015–2016. Lei Wang would also like to thank Prof. Jung Han from Yale University for facility assistance and Prof. Junjie Li from the Institute of Physics of the Chinese Academy of Sciences for TEM sample preparation. Dr. Lei Wang also acknowledges Dr. Jian Gao from Rensselaer Polytechnic Institute, Dr. Chao Wang and Dr. Yumiao Lyu from the Institute of Physics of the Chinese Academy of Sciences, and Dr. Luoning Ma from Johns Hopkins University for technical assistance.

Notes and references

1 J. A. Rogers, M. G. Lagally and R. G. Nuzzo, *Nature*, 2011, **477**, 45–53.
2 W. Y. Nie, H. H. Tsai, R. Asadpour, J. C. Blancon, A. J. Neukirch, G. Gupta, J. J. Crochet, M. Chhowalla, S. Tretiak, M. A. Alam, H. L. Wang and A. D. Mohite, *Science*, 2015, **347**, 522–525.
3 T. Das, X. Chen, H. Jang, I. K. Oh, H. J. Kim and J. H. Ahn, *Small*, 2016, **12**, 5720–5727.
4 S. Nakamura, T. Mukai and M. Senoh, *Appl. Phys. Lett.*, 1994, **64**, 1687–1689.
5 J. Xia, X. Huang, L. Z. Liu, M. Wang, L. Wang, B. Huang, D. D. Zhu, J. J. Li, C. Z. Gu and X. M. Meng, *Nanoscale*, 2014, **6**, 8949–8955.
6 H. Kaneko, T. Minegishi, M. Nakabayashi, N. Shibata, Y. B. Kuang, T. Yamada and K. Domen, *Adv. Funct. Mater.*, 2016, **26**, 4570–4577.
7 J. W. Elam and S. M. George, *Chem. Mater.*, 2003, **15**, 1020–1028.
8 H. Saito, V. Zayets, S. Yamagata and K. Ando, *Phys. Rev. Lett.*, 2003, **90**, 4.
9 J. Song, G. Yuan, K. Xiong, B. Leung and J. Han, *Cryst. Growth Des.*, 2014, **14**, 2510–2515.
10 J. Yan, X. Fang, L. Zhang, Y. Bando, U. K. Gautam, B. Dierre, T. Sekiguchi and D. Golberg, *Nano Lett.*, 2008, **8**, 2794–2799.
11 A. Bourret, *Appl. Surf. Sci.*, 2000, **164**, 3–14.
12 H. Yang, W. Wang, Z. Liu and G. Li, *CrystEngComm*, 2013, **15**, 7171–7176.
13 X. Wu, P. Jiang, Y. Ding, W. Cai, S. Xie and Z. L. Wang, *Adv. Mater.*, 2007, **19**, 2319–2323.
14 J. Zhu, X. Wei, Y. Zhang and Y. Li, *J. Appl. Phys.*, 2006, **100**, 104106.
15 Z. W. Wang, L. L. Daemen, Y. S. Zhao, C. S. Zha, R. T. Downs, X. D. Wang, Z. L. Wang and R. J. Hemley, *Nat. Mater.*, 2005, **4**, 922–927.
16 S. Nakamura, Y. Yamada and T. Taguchi, *J. Cryst. Growth*, 2000, **214**, 1091–1095.
17 X. S. Fang, Y. Bando, M. Y. Liao, U. K. Gautam, C. Y. Zhi, B. Dierre, B. D. Liu, T. Y. Zhai, T. Sekiguchi, Y. Koide and D. Golberg, *Adv. Mater.*, 2009, **21**, 2034–2039.
18 Q. Sun, Y. A. Wang, L. S. Li, D. Y. Wang, T. Zhu, J. Xu, C. H. Yang and Y. F. Li, *Nat. Photonics*, 2007, **1**, 717–722.
19 L. X. Shao, K. H. Chang and H. L. Hwang, *Appl. Surf. Sci.*, 2003, **212**, 305–310.
20 C. Ma, D. Moore, J. Li and Z. L. Wang, *Adv. Mater.*, 2003, **15**, 228–231.
21 M. Misao and N. Takashi, *Jpn. J. Appl. Phys.*, 1993, **32**, 743.
22 X. S. Fang, C. H. Ye, L. D. Zhang, Y. H. Wang and Y. C. Wu, *Adv. Funct. Mater.*, 2005, **15**, 63–68.
23 X. Huang, M. Wang, M.-G. Willinger, L. Shao, D. S. Su and X.-M. Meng, *ACS Nano*, 2012, **6**, 7333–7339.
24 D. H. Ha, A. H. Caldwell, M. J. Ward, S. Honrao, K. Mathew, R. Hovden, M. K. A. Koker, D. A. Muller, R. G. Hennig and R. D. Robinson, *Nano Lett.*, 2014, **14**, 7090–7099.
25 X. Huang, M. G. Willinger, H. Fan, Z. L. Xie, L. Wang, A. Klein-Hoffmann, F. Girgsdies, C. S. Lee and X. M. Meng, *Nanoscale*, 2014, **6**, 8787–8795.
26 M. S. Akhtar, M. A. Malik, Y. G. Alghamdi, K. S. Ahmad, S. Riaz and S. Naseem, *Mater. Sci. Semicond. Process.*, 2015, **39**, 283–291.
27 Y.-Q. Yu, L.-B. Luo, Z.-F. Zhu, B. Nie, Y.-G. Zhang, L.-H. Zeng, Y. Zhang, C.-Y. Wu, L. Wang and Y. Jiang, *CrystEngComm*, 2013, **15**, 1635–1642.
28 M. Safari, Z. Izadi, J. Jalilian, I. Ahmad and S. Jalali-Asadabadi, *Phys. Lett. A*, 2017, **381**, 663–670.
29 H. Lashgari, A. Boochani, A. Shekaari, S. Solaymani, E. Sartipi and R. T. Mendi, *Appl. Surf. Sci.*, 2016, **369**, 76–81.
30 C. L. Tan, Z. Y. Zeng, X. Huang, X. H. Rui, X. J. Wu, B. Li, Z. M. Luo, J. Z. Chen, B. Chen, Q. Y. Yan and H. Zhang, *Angew. Chem., Int. Ed.*, 2015, **54**, 1841–1845.
31 G. X. Zhu, J. Yang, C. L. Bao, X. Y. Zhang, Z. Y. Ji, S. K. Wu and X. P. Shen, *J. Colloid Interface Sci.*, 2016, **468**, 136–144.
32 J. Jie, W. Zhang, I. Bello, C.-S. Lee and S.-T. Lee, *Nano Today*, 2010, **5**, 313–336.
33 X. Huang, M.-G. Willinger, H. Fan, Z.-l. Xie, L. Wang, A. Klein-Hoffmann, F. Girgsdies, C.-S. Lee and X.-M. Meng, *Nanoscale*, 2014, **6**, 8787–8795.
34 R. Hull and J. C. Bean, *Crit. Rev. Solid State Mater. Sci.*, 1992, **17**, 507–546.
35 Y. Chen and J. Washburn, *Phys. Rev. Lett.*, 1996, **77**, 4046–4049.

36 M. J. Hytch, E. Snoeck and R. Kilaas, *Ultramicroscopy*, 1998, **74**, 131–146.
37 R. People and J. C. Bean, *Appl. Phys. Lett.*, 1985, **47**, 322–324.
38 S. S. Lo, T. Mirkovic, C.-H. Chuang, C. Burda and G. D. Scholes, *Adv. Mater.*, 2011, **23**, 180–197.
39 W. Chen, N. Zhang, M. Y. Zhang, X. T. Zhang, H. Gao and J. Wen, *CrystEngComm*, 2014, **16**, 1201–1206.